Proceedings of the 3rd International Conference on Materials Chemistry and Environmental Engineering (CONF-MCEE 2023), Part II
DOI: 10.54254/2755-2721/7/20230557

Plastic deformation of Ag/MgO interface system during tensile fracture: A molecular dynamics study

Xueqiong Fu

Shenzhen Institute of Advanced Electronic Materials, Shenzhen Institute of Advanced Technology, Chinese Academy of Sciences, Shenzhen 518055, China

xq.fu@siat.ac.cn

Abstract: Fracture experiments on layered metal-ceramic composites show that the plastic dissipation in the metal near the crack tip accounts for most of the macroscopic fracture toughness. In this work we studied the microscopic plastic deformation mechanisms of Ag/MgO interface systems using molecular dynamics (MD) method. As tensile strain increases, lattice dislocations nucleate at interface misfit dislocations and propagate in metal layer. The formation of immobile Hirth dislocations in Ag causes hardening. As the metal layer increases, the yield strength decreases and the hardening range is shortened. Large interface area increases the degree of inhomogeneity of dislocation motion and interface fracture behavior, leading to decreased interface yield strength.

Keywords: Metal/Ceramic Interface, Interface Fracture, Plastic Deformation, Molecular Dynamics.

1. Introduction

Metal-ceramic interfaces widely exist in many technical applications such as microelectronic packaging [1,2] and oxide coatings on metals [3,4]. Interface adhesion is closely associated with the service life of relevant structures and devices. Interface strength and work of separation are two key parameters characterizing the adhesive properties of the interface and depend mainly on the interface structure and plastic deformation in metal. Fracture experiments on layered metal-ceramic composites show the macroscopic fracture toughness of the interface is nearly 1000 times higher than that of the interfacial work of separation at atomic scale [5,6]. Such a huge energy difference is mainly ascribed to the plastic dissipation in metal. A better understanding of the correlation between plastic deformation mechanisms and mechanical properties of the interface can help in the nanostructural design of metal/ceramic interfaces.

Interface fracture is essentially the fracture of interfacial atomic bonds, and the strength and quantity of interfacial chemical bonds directly affect the tensile strength of the interface. Plasma pretreatment on nanoscale Al/AlN and Cu/AlN interfaces show rearrangement of metal to the ceramic due to plastic deformation near the interface [7], which enhances interface adhesion. Furthermore, due to the differences in lattice types and lattice constants, most metal/ceramic interfaces have defects, such as misfit dislocations and vacancies. These defects not only act as natural dislocation nucleation sites, but also hinder the transmission of dislocations from metals to ceramics [8]. Due to the complexity of

DOI: 10.54254/2755-2721/7/20230557

metal/ceramic interfaces and lack of accurate description of metal/ceramic interface systems, studies on the plastic deformation mechanisms associated with metal/ceramic interface fracture are limited [8,9].

In this work, we performed molecular dynamics simulations to study the plastic deformation mechanism of metal/ceramic (Ag/MgO) interface systems under tensile loading. The interface structure and dislocation reaction were investigated numerically by dislocation analysis. In particular, the influence of metal layer thickness and interface area were explored.

2. Models and methods

Figure 1 shows the simulation model of the semi-coherent Ag/MgO interface system. The interface model adopts the cube-on-cube structure and the orientation relationship is $[100]_{Ag} \parallel [100]_{MgO}$ (x-axis), [010]Ag || [010]MgO (y-axis), [001]Ag || [001]MgO (z-axis, interface normal) [10]. Periodic boundary conditions were applied in all directions. To avoid the spurious slab-slab interactions along the z-axis, a sufficiently thick vacuum layer is inserted between the Ag slab and MgO slab.

According to the lattice misfit between MgO and Ag ($a_{\mathrm{MgO}} = 4.32$ Å, $a_{\mathrm{Ag}} = 4.10$ Å), the misfit dislocation network was constructed by establishing a $(20 \times 20) : (19 \times 19)$ interface model, where 20 and 19 are the numbers of Ag lattices and MgO lattices along the direction parallel to the interface in the minimum periodic interface structure. To study the effect of interface area, an interface model four times larger than this minimal periodic structure was constructed. The thickness of MgO slab L_z^{MgO} is kept at 3.5 nm, and the thickness of the Ag slab L_z^{Ag} varies from 3.3 nm to 8.2 nm.

For Ag/MgO interface system, the interface potential is of the modified Rahman-Stillinger-Lemberg (RSL2) form:

$$\Phi_{\mathrm{pair}}(r) = D_0 e^{y\left(1-\frac{r}{R_0}\right)} + \frac{a_1}{1+e^{b_1(r-c_1)}} + \frac{a_2}{1+e^{b_2(r-c_2)}} + \frac{a_3}{1+e^{b_3(r-c_3)}} \quad (1)$$

the specific potential parameters for interface and bulk potentials can be referred to Ref. [11,12].

The initial interface structure was statically relaxed by energy minimization through the conjugate gradient (CG) algorithm. Then the interface structure was dynamically relaxed through NPT ensemble at zero pressure and 1K. After relaxation, the summation of the transverse stresses approaches zero (< 200 MPa). During the tensile loading process, the MgO atoms in the bottom layer were fixed and the Ag atoms in the top layer move along the z-axis at a fixed velocity v. To avoid the shock wave effect accompanied with displacement loading, initial velocities distributed linearly from 0 to v were applied to the mobile atoms in the middle. Five tensile strain rates were studied: 1×10^8 s^{-1}, 5×10^8 s^{-1}, 1×10^9 s^{-1}, 1.5×10^9 s^{-1}, 2×10^9 s^{-1}. The open source MD program LAMMPS [13] was used for simulations. The evolution of the atomic configurations was visualized by using OVITO [14]. The centro-symmetry parameter (CSP) [15] was calculated to characterize defect atoms (e.g. dislocation, stacking fault or surface).

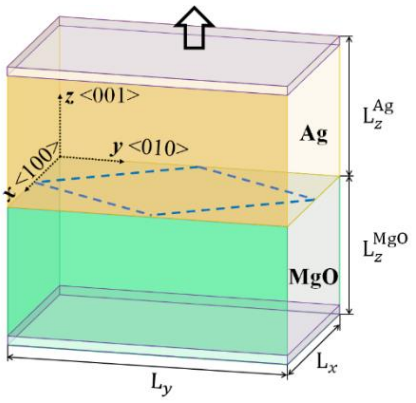

Figure 1. The simulation model of semi-coherent Ag/MgO interface system used in tensile loading. The blue dashed lines represent the interface misfit dislocations.

DOI: 10.54254/2755-2721/7/20230557

3. Results

3.1. Tensile fracture mechanism

Figure 2(a) shows the tensile stress-strain curve and changes of dislocation length of Ag/MgO interface system. The atomic structures corresponding to different key points on the stress-strain curve are shown in Figure 2(b). Due to the difference in elastic constants C_{11} between Ag (122.2 GPa [16]) and MgO (294 GPa [16]), the dislocations nucleated in the Ag slab do not transmit to the MgO slab. Figure 2(b) shows only the defect atoms in Ag slab.

In the initial elastic deformation stage, the stress increases linearly with the increase of strain until the stress reaches the first peak of 4.8 GPa (Point A). Lattice dislocations nucleate at interface misfit dislocations and propagate in Ag with the increase of strain. The lattice dislocations deposit on the upper surface of Ag and these defects become new sources of dislocation. Correspondingly, the total length of dislocation increases rapidly and stress drops from 4.8 GPa to 4.1 GPa (Point A to Point B). Interfacial misfit dislocations, lattice dislocations and deposited dislocations interact to form the Hirth dislocations in Ag:

$$\frac{1}{6}[112]+\frac{1}{6}[1\bar{1}\bar{2}]=\frac{1}{3}[100] \tag{2}$$

In FCC metals the slip system is 1/2{111}[110]. 1/3[100] are stable dislocation segments on crystallographic directions ([100]) that are not slip directions. These immobile dislocations become the abundant barrier to nearby mobile dislocations [17]. As a result, hardening occurs and the total length of dislocation remains basically the same (Point C to Point D). Note that at the interface yield strength (Point D), the interfacial Ag atoms rearrange and the effective interface area (Ag on O site) is expanded—defective atoms exist only in the dislocation node regions (Point D).

With further increase in tensile strain, microcracks form at one of the misfit dislocation nodes, forming new free surfaces. The Hirth dislocations resolve into Shockley dislocations (1/6[112]), which are attracted to the free surfaces and escape from the free surfaces. The interface separation area rapidly expands to the entire interface area and the interface loses carrying capacity. Finally, the interface is completely separated and the stress is reduced to zero (Point D to Point F).

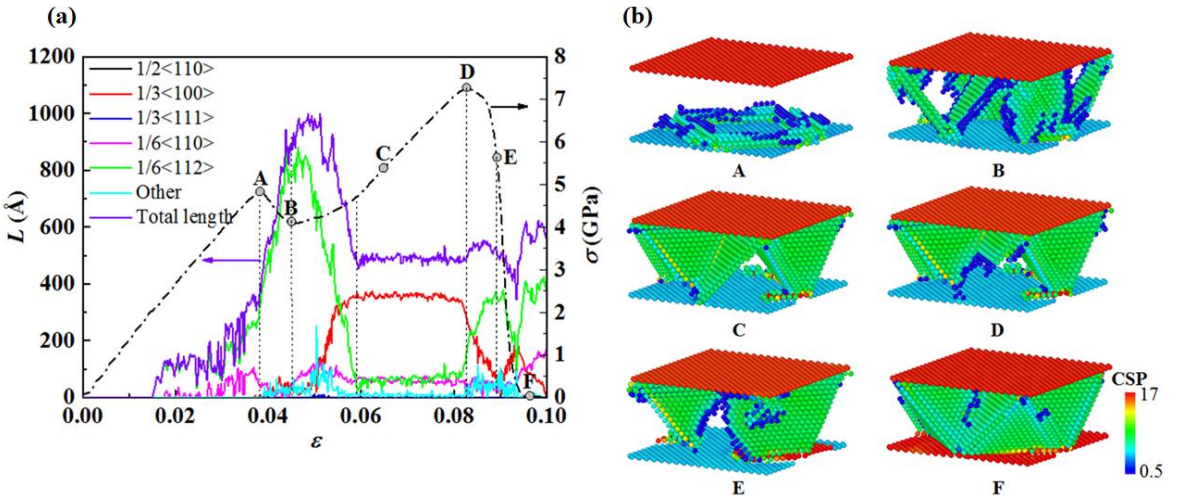

Figure 2. (a) Tensile stress-strain curve and the corresponding changes of dislocation length of Ag/MgO interface system ($\dot{\varepsilon}$ = 1×10^9 s^{-1}). (b) Dislocation activities in the Ag slab for 3.3 nm Ag/3.5 nm MgO interface system. Defect atoms are colored according to the centro-symmetry parameter (CSP).

DOI: 10.54254/2755-2721/7/20230557

3.2. *Effect of layer thickness*

For Ag/MgO interface system studied in this work dislocation motion occurs mainly in metals [9]. To explore the effect of metal layer thickness on tensile fracture mechanisms of Ag/MgO interface, the thickness of Ag layer was increased from 3.3 nm to 8.2 nm while the thickness of MgO layer was kept at 3.5 nm.

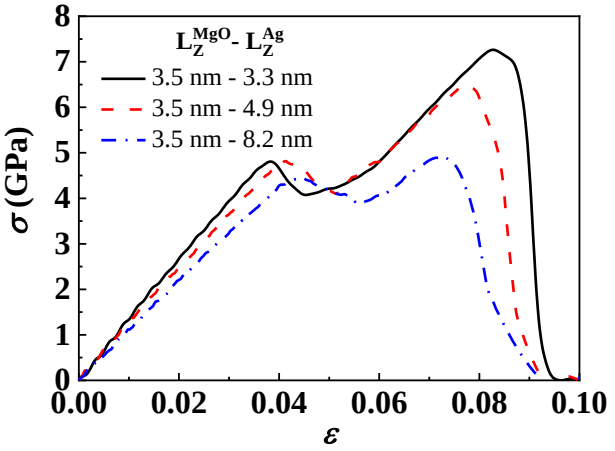

Figure 3. Tensile stress-strain curves of Ag/MgO interface models with different Ag layer thicknesses ($\dot{\varepsilon} = 1\times10^9$ s^{-1}).

Figure 3 shows the stress-strain curves of the three Ag/MgO interface systems with different Ag layer thickness. Overall, three curves show the same trend while the degree of hardening varies. First, the thicker the metal layer thickness, the lower the effective elastic modulus of the interface system. Since the elastic modulus of Ag is much lower than that of MgO, the effective elastic modulus decreases with increasing thickness of metal layer. Second, the yield strength decreases with increasing Ag layer thickness. The hardening rate is almost insensitive to the layer thickness and three models all fracture completely when the tensile strain reaches 0.1.

3.3. *Effect of interface area*

Due to the initial defects such as voids and pre-existing dislocations, the metal/ceramic interface is generally not a regular periodic structure [18]. Dislocation motion and interaction may be highly inhomogeneous. We study the fracture mechanisms of Ag/MgO interface with larger interface area (16.4 nm × 16.4 nm). The model thickness is 3.5 nm (MgO)/3.3 nm (Ag). To ensure the interface misfit dislocations, lattice dislocations, and deposited dislocations fully interact with each other, MD simulations were performed at a lower strain rate of 5×10^8 s^{-1}.

Figure 4(a) shows the tensile stress-strain curves of Ag/MgO interface model with different interface areas. Compared with the interface model with small interface area (8.2 nm × 8.2 nm), the fracture behavior of interface model with large interface area (16.4 nm × 16.4 nm) is more complex. The interface defects are mainly located near the interface misfit dislocation lines (Figure 4(b)), and atoms at these regions become natural dislocation nuclei. At the first critical strain of 0.037 (Point A), lattice dislocations nucleate from interface misfit dislocations and glide along the {111} slip plane. Correspondingly, stress begins to drop. Dislocations move to the upper bound of Ag slab and reflect back. The reflected dislocations move to and deposite at the interface. These deposited dislocations become new dislocation nuclei (Point B). The formation of immobile Hirth dislocations in silver causes hardening phenomenon (Point B to Point C). At the second critical strain of 0.058 (Point C), local separation occurs at the interface and new free surfaces are formed, as shown by the red atoms in Figure 4(c) with high centro-symmetry values. As the tensile deformation increases, the local microcracks expand along the interface and the stress drops from 4.78 GPa to 3.47 GPa (Point C to Point D). Since the unfractured area of the interface is still capable to bear tensile load, the stress increases slightly and the second hardening phenomenon occurs (Point D to Point E). Finally, the local microcracks spread to the whole interface and the stress drops to zero (Point E to Point F). In short, large interface area increases the degree of inhomogeneity of both dislocation motion in metal

DOI: 10.54254/2755-2721/7/20230557

and interface fracture behavior, which ultimately results in a decrease in interfacial yield strength (6.8 GPa to 4.7 GPa).

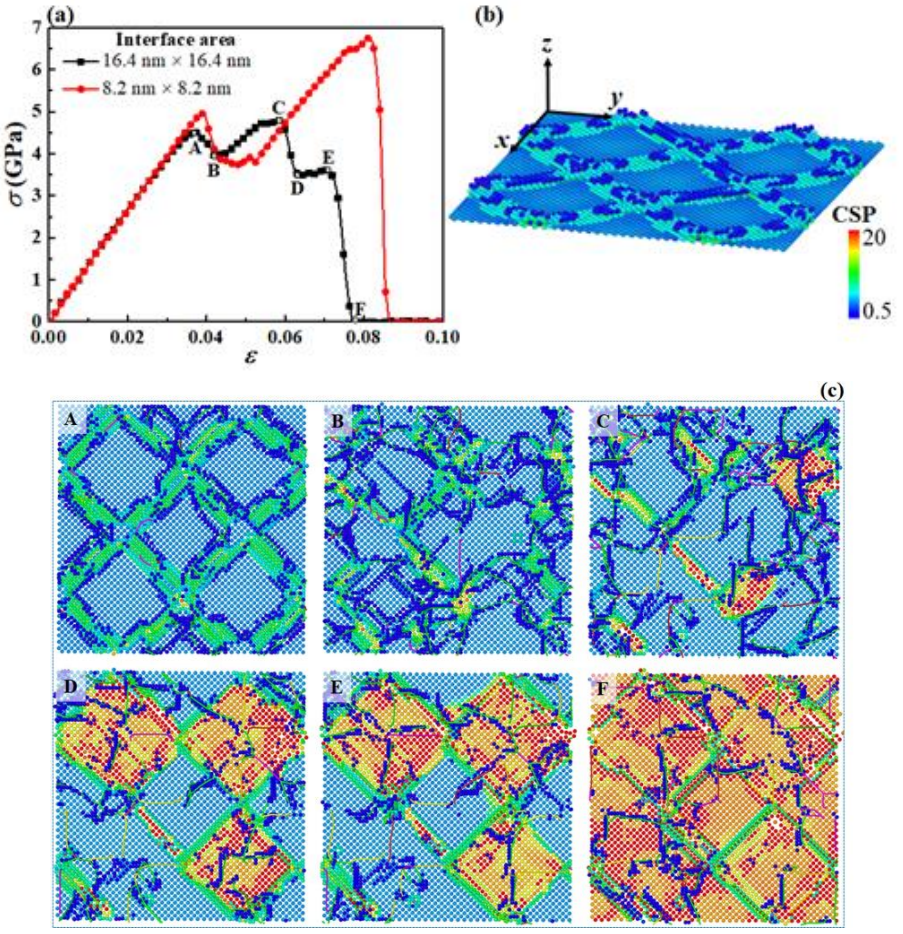

Figure 4. (a) Tensile stress-strain curves of Ag/MgO interface systems with different interface areas ($\dot{\varepsilon} = 5\times10^{8}$ s^{-1}). (b) Atomic structures of the equilibrium Ag/MgO interface. Defect atoms in the Ag layer are colored according to the centro-symmetry parameter (CSP). (c) Atomic structures corresponding to the key points in the stress-strain curve in (a).

4. Conclusion

Molecular dynamics simulations were performed to study the plastic deformation mechanisms during tensile fracture of Ag/MgO interface systems. After interface yields, the interaction of partial dislocation, interface deposited dislocation and interface misfit dislocation in the metal slab leads to strain hardening. The interface yield strength decreases with increasing metal layer thickness. The increase in interface area causes inhomogeneous distribution of dislocation movement and fracture area. The large interface system undergoes two hardening processes and the tensile strength of the interface is reduced compared with the interface model with small interface area.

5. Acknowledgments

This work was supported by the Shenzhen Post-doctoral Funding (E2915).

DOI: 10.54254/2755-2721/7/20230557

References

[1] Wikstrom A, Gudmundson P, Suresh S 1999 *J. Mech. Phys. Solids* **47** (5) 1113-1130
[2] Shen Y L, Suresh S, Blech I A 1996 *J. Appl. Phys.* **80** (3) 1388-1398
[3] Kumar V, Kandasubramanian B 2016 *Particuology* **27** 1-28
[4] Smith J, Scheibel J, Classen D, Paschke S, Elbel S, Fick K, Carlson D 2016 *J. Eng. Gas Turbines Power* **138** (3)
[5] Elssner G, Korn D, Ruhle M 1994 *Scr. Metall. Mater.* **31** (8) 1037-1042
[6] Korn D, Elssner G, Fischmeister H F, Ruhle M 1992 *Acta Metall. Mater.* **40** S355-S360
[7] Jang K B, Mhin S, Lim S C, Song Y S, Lee K H, Park S K, Moon, Kyoung I, Lee S H, Hyun S K 2018 *J. Electron. Mater.* **48** (1) 72-78
[8] Salehinia I, Shao S, Wang J, Zbib H M 2015 *Acta Mater.* **86** 331-340
[9] Damadam M, Shao S, Ayoub G, Zbib H M 2017 *J. Mater. Sci* **53** (8) 5604-5617
[10] Trampert A, Ernst F, Flynn C P, Fischmeister H F, Ruhle M 1992 *Acta Metall. Mater.* **40** S227-S236
[11] You X M, Liang L H, Wei Y G 2018 *Comp. Mater. Sci.* **142** 277-284
[12] Fu X Q, Liang L H, Wei Y G 2018 *Comp. Mater. Sci.* **155** 116-128
[13] Plimpton S 1995 *J. Comput. Phys.* **117** (1) 1-19
[14] Stukowski A 2010 *Modell. Simul. Mater. Sci. Eng.* **18** (1) 015102
[15] Kelchner C L, Plimpton S J, Hamilton J C 1998 *Phys. Rev. B* **58** (17) 11085-11088
[16] Levy M, Bass H E, Stern R R 2001 *Handbook of Elastic Properties of Solids Liquids and Gases vol. 2*. Academic Press: New York
[17] Hirth J P, Lothe J 1982. *Theory of Dislocations*. Krieger Publishing Company: Malabar, FI.
[18] Meltzman H, Mordehai D, Kaplan W D 2012 *Acta Mater.* **60** (11) 4359-4369